Supporting Information

Gilaie-Dotan et al. 10.1073/pnas.1414974112

Case Descriptions: Additional Details

Left Hemisphere Lesions.

EL case description. EL suffered a left posterior cerebral artery (PCA) infarct affecting the medial temporal lobe and occipital lobe as revealed by a 3T MRI scan (Fig. 3). EL has participated in many previous studies, which provide detailed description of her abilities and impairments (1–7). Briefly, these earlier studies revealed that she has pure alexia as well as some difficulty in object and face recognition. She worked as a reading specialist before her stroke.

GB case description. GB suffered a PCA stroke. An MRI scan performed 3 y poststroke revealed a lesion affecting two-thirds of the left temporal lobe and the inferior aspect of the left occipital lobe (Fig. 3). She suffers from pure alexia and, as uncovered in previous studies (5–7), she has some mild impairment in object and face recognition, too. GB worked as a graphic artist before her stroke.

SH case description. SH suffered from a lesion affecting left temporo-occipital structures and the left thalamus, compatible with a left PCA infarct (Fig. 3). He suffers from pure alexia and, as uncovered in previous studies (6, 7), he has mild impairments in face and object recognition. SH worked as a lawyer before his stroke.

Right Hemisphere Lesions.

SM case description. SM sustained a closed head injury in a motor vehicle accident at the age of 18 and recovered well after rehabilitation, aside from a persisting visual agnosia and prosopagnosia. Recent neuroimaging (8) revealed a circumscribed lesion in the posterior portion of the right lateral fusiform gyrus. Further details of his medical and neuropsychological history can be found in previous studies (5, 6, 9–12). SM works in a photography studio.

CR case description. CR suffered from a right temporal lobe abscess with a complicated medical course, including a history of Group A toxic shock syndrome, pneumonia, cardiac arrest, candida bacteremia, and metabolic encephalopathy in May 1996, ∼15 y before his participation in this study. MR scans reveal a right temporal lobe lesion consistent with acute microabscesses of the right temporal lobe and medial occipital lobe, and there are small lacunae in the left hemisphere as well. CR has participated in several previous studies (5, 6, 9, 10, 13) that highlight his visual perceptual deficits, which include impaired recognition of objects and of faces. CR completed community college and now runs a restaurant.

EC case description. EC was tested 4 y after suffering an infarction. The radiology report states that there is low attenuation at the right temporal lobe and right occipital lobe posteriorly, consistent with a right PCA infarct. She showed difficulties in both face and object recognition on screening tests conducted before these experiments (5).

Additional Experimental Details

Experiment 1: Additional Experimental Details. This experiment has been described in detail elsewhere (14, 15). Biological motion animations were created by videotaping an actor performing various activities, and encoding only the joint positions in digitized videos (16). In the movies, the joints were represented by 12 small white points against a black background (Fig. 1*A*; for an animated example, see Movies S2 and S3).

Each animation consisted of 20 distinct frames and was displayed for 0.5 s (16.5-ms interframe interval, 60 Hz). The final frame then remained visible for 0.3 s, after which the animation looped from the beginning. Because a joint could become occluded by other body parts during an action, some points were briefly invisible at times.

For each of the animations, the matched spatially scrambled animation was created by scrambling the starting positions of the 12 points while keeping the motion trajectories of each point unchanged. The starting positions of the scrambled points were chosen randomly within a region so that the total area encompassed by the scrambled animation was similar to that of the original nonscrambled biological animation (Fig. 1*A*).

Experiment 2: Additional Experimental Details.

Stimuli. This experiment included the seven animations from Exp. 1 and five additional ones (climbing stairs, skipping rope, kicking leftward with right leg, bending down, and pitching). All of the animations were created in the same manner as described in Exp. 1. For each animation, a spatially scrambled matched-version animation was created as described in Exp. 1. As in Exp. 1, a variable number of noise points, each with a motion trajectory as one of the points from the target biological motion animation, were also presented on each trial of the perceptual threshold assessment (in each trial, all of the noise point motion trajectories were from the same animation), and the initial spatial location of the noise points was determined randomly.

The PLD that was presented centrally in each trial subtended ∼4° × 8° visual angle when viewed from 55 cm while the region populated by the PLD and the noise points together was ∼8° × 12° visual angle. On each trial, the target (or nontarget) PLD was presented at a randomly jittered location within a 2.2° radius from the center of the screen. Stimuli were presented and responses recorded using Matlab (Mathworks) and the Psychophysics Toolbox v2.54 (17, 18).

Procedure. The experiment started with assessing action recognition of unmasked PLD animations. The participants were not informed about what they were about to view and were instructed to describe what they saw. Following this phase, we assessed perceptual thresholds. Each participant completed a practice block that included 16 trials with a range of predetermined number of noise points (ranging from 0 to 40). The practice was followed by the main experimental block, which included 60 trials in which the number of noise points was determined in an adaptive manner, contingent on performance, beginning with 10 noise points. Varying the number of noise points enabled us to measure biological motion-detection thresholds at which each participant performed at 75% accuracy (19), and this was done using the same Bayesian adaptive paradigm as in Exp. 1 (QUEST). The task became more difficult with an increasing number of noise points.

Each trial started with a white fixation cross displayed at the center of the screen for 750 ms, after which the PLDs were presented along with noise points. The animations were repeated continuously until a response was given. After each response, a visual feedback cue appeared for 750 ms (green fixation cross for correct, red for incorrect).

Data analysis. Thresholds were calculated for each patient and for each of the control participants, and data (thresholds and response times) were analyzed as in Exp. 1.

SI Results

Experiment 1: Additional Results. We have now also conducted a set of comparisons of ventral patient group vs. matched control group using the perceptual thresholds measured in Exp. 1. In each comparison (two-tailed t test assuming unequal variance), we

randomly picked for each patient one control from his or her control group to serve as the matched control for that test so that the groups were matched in size. We then redid this control sampling 10 times. In 6 of the 10 statistical comparisons, there was no significant difference between the ventral patients group and the age-matched control group (*P*s = 0.502, 0.107, 0.802, 0.197, 0.116, 0.158); in three of the runs there was a borderline effect ($0.05 < P < 0.1$); and in one run there was a significant effect between the groups ($P < 0.05$).

These results are reassuring in showing that in most cases the ventral patients are indeed within the norm of healthy age-matched controls, even at a group level. Also, because it is typical for a group of (any type of) brain-damaged patients to perform significantly more poorly than a group of age-matched controls (*Results*), that we see borderline effects in some comparisons is perhaps not surprising. In addition, given the small sample size, the variability may not be surprising either.

Experiment 2: Additional Results. We also carried out the same group vs. group statistical comparisons that are described above (the set of 10 comparisons for ventral patient group vs. matched control group) with the perceptual thresholds derived in Exp. 2. In 10 of the 10 comparisons, the performance of the patients' group did not significantly differ from that of the matched control group (*P*s = 0.327, 0.212, 0.547, 0.132, 0.911, 0.579, 0.153, 0.447, 0.608, 0.212). These results further confirm our finding that the ventral patients perform normally on biological motion perception, as evident in a different paradigm.

Ventral Visual Patients' Structural Image Acquisition

EL. EL's anatomical MR scans were acquired at the Brain Imaging Research Center Pittsburgh on a Siemens Allegra MRI 3T scanner using a head coil, when she was 60 y old, approximately 1 y before her participation in this study and 14 y after her injury. The scan acquired 192 MPRAGE sagittal slices (1-mm thickness, inplane resolution of 1×1 mm^2, matrix = 256×256, repetition time 1,740 ms, echo time 3.04 ms, inversion time 1,000 ms, flip angle = 8°).

GB. GB's MR clinical structural scans were acquired on a 1.5T GE Genesis Signa MR scanner equipped with a head coil, ∼3 y before her participation in this study. These included 23 axial T2 images (slice thickness = 5.5 mm, 7 mm gap, image size 512×512, pixel spacing 0.42968×0.42968 mm^2, echo time = 96.512 ms, no. of averages = 2, flip angle = 90°).

SH. SH's CT clinical structural scans were acquired on a Siemens SOMATOM Sensation 4 CT scanner when he was 63 y old, and ∼6 y before his participation in this study. These included axial images with slice thickness/overlap of 5.0/2.5 mm.

SM. SM's MRI structural scans were acquired with identical parameters to those of EL's (see above) at the Brain Imaging Research Center Pittsburgh when he was 35 y old. This was 17 y after his injury and ∼2 y before his participation in this study (for details, see ref. 8).

CR. CR's MRI structural scans were acquired at the Magnetic Resonance Research Center, University of Pittsburgh Medical Center on a 1.5T Signa whole-body scanner (General Electric Medical Systems), ∼3 y after he had metabolic encephalopathy and ∼12 y before his participation in this study. This included 124 slices of 1.5-mm thickness with an inplane resolution of 0.9375×0.9375 mm^2, matrix of 256×256.

EC. EC's CT clinical structural scans were acquired on a GE Medical Systems LightSpeed QX/i CT scanner when she was 40 y old, and ∼8 y before her participation in this study. These included 34 axial images without contrast with slice thickness of 2.5 mm (through the posterior fossa) and 7.5 mm (from the posterior fossa to the vertex), 512×512 image size, and pixel spacing of 0.449219×0.449219 mm^2.

Lesion-Tracing Criteria

We used an established procedure and most of these details are published elsewhere (5). We describe below specific modifications we made to document the lesion of each patient, where necessary.

EL. Because the average intensity values varied across each structural image regardless of the lesion (e.g., between anterior and posterior regions, or right and left hemispheres), the definition of the lesioned tissue was not based solely on absolute intensity values, and relative local differences were considered as well. Instead, the definition of the lesioned tissue also took into account abrupt local changes in intensities between lesioned and adjacent healthy tissue, and continuity of abnormal lesioned tissue. Locally, lesioned tissue always had substantially lower values of intensity than healthy tissue. In most parts of EL's brain and around the lesion, healthy tissue-intensity values ranged from 200 to above 350, whereas lesioned tissue-intensity values ranged from 54 to 170. However, in specific locations the value, 170, was considered healthy tissue (adjacent to value of 117 of a lesioned tissue). We provide lesion size estimates based on local intensity variations and continuity assessment, and also a more conservative estimation based on intensity values <150 in the predefined lesion zone (Table 3).

SM. SM's structural images also revealed local variations in intensity values; thus, as with EL, we delineated the lesion based on intensity values, continuity of the lesioned tissue, and abrupt changes in local intensity values between the lesion and adjacent healthy tissue. Common values for healthy tissue were above 200 to even above 350; however, locally healthy tissue could have value of 171. Lesioned tissue typically had values ranging from as low as 60 to values around 150; however, locally, values of 160 or 174 could be attributed to lesioned tissue. We provide the lesion size estimate according to the criteria laid out above, along with a conservative estimate for the lesion when lesioned intensities are <160.

CR. Because CR's lesion is of a different etiology than that of EL and SM, the lesion delineation criteria were different. CR has a definitive lesion in the right temporal lobe (see above) that is evident and confirmed by an expert neuroradiologist in the past and during the present study. In addition, there are foci of petechial hemorrhage seen along the gray/white junction at multiple areas that appear as a very dark center (intensity values of below 35) bordered by very bright intensity tissue (intensity above 120). Healthy tissue in CR's structural images had intensity values of 55–95. There are, however, some small foci of enhancement in the left hemisphere (perhaps resolved abscesses) and so we adopt a conservative approach here and leave open the possibility of additional left hemisphere insult.

GB, EC, and SH. Lesioned tissue in GB's, EC's, and SH's original clinical structural images were used to guide delineation in a normalized MNI canonical brain. GB's original DICOM images were loaded into MATLAB (Mathworks), where intensity values of lesioned tissue were above 0.5 and healthy tissue intensity values were below 0.4. Because of technical issues with MATLAB reading EC's DICOM images, EC's structural images were loaded into MicroDicom (www.microdicom.com) and then exported to bitmap images. Typically, lesioned tissue intensity values were below 105 and healthy tissue values were above 110. In the lesion delineation process we also took into account (as with the other patients) continuity of the lesioned tissue and

abrupt intensity changes between the lesion and adjacent healthy tissue. After the lesion tracing in the original images detailed above, an approximated corresponding delineation was carried out onto a single subject T1 SPM MNI-normalized template. Following that process, we manually interpolated each lesion into a continuous lesion in a conservative manner. This process was achieved in MRIcroN software (www.mricro.com), where the originally traced lesioned volume (in axial sections) was then filled in manually in the orthogonal section planes (sagittal and coronal) by linear interpolation (Fig. S1).

1. McKeeff TJ, Behrmann M (2004) Pure alexia and covert reading: Evidence from Stroop tasks. *Cogn Neuropsychol* 21(2):443–458.
2. Mycroft RH, Behrmann M, Kay J (2009) Visuoperceptual deficits in letter-by-letter reading? *Neuropsychologia* 47(7):1733–1744.
3. Montant M, Behrmann M (2001) Phonological activation in pure alexia. *Cogn Neuropsychol* 18(8):697–727.
4. Behrmann M, Nelson J, Sekuler EB (1998) Visual complexity in letter-by-letter reading: "Pure" alexia is not pure. *Neuropsychologia* 36(11):1115–1132.
5. Gilaie-Dotan S, et al. (2013) The role of human ventral visual cortex in motion perception. *Brain* 136(Pt 9):2784–2798.
6. Behrmann M, Plaut DC (2014) Bilateral hemispheric processing of words and faces: Evidence from word impairments in prosopagnosia and face impairments in pure alexia. *Cereb Cortex* 24(4):1102–1118.
7. Habekost T, Petersen A, Behrmann M, Starrfelt R (2014) From word superiority to word inferiority: Visual processing of letters and words in pure alexia. *Cogn Neuropsychol* 31(5-6):413–436.
8. Konen CS, Behrmann M, Nishimura M, Kastner S (2011) The functional neuroanatomy of object agnosia: A case study. *Neuron* 71(1):49–60.
9. Gauthier I, Behrmann M, Tarr MJ (1999) Can face recognition really be dissociated from object recognition? *J Cogn Neurosci* 11(4):349–370.
10. Marotta JJ, Genovese CR, Behrmann M (2001) A functional MRI study of face recognition in patients with prosopagnosia. *Neuroreport* 12(8):1581–1587.
11. Behrmann M, Kimchi R (2003) What does visual agnosia tell us about perceptual organization and its relationship to object perception? *J Exp Psychol Hum Percept Perform* 29(1):19–42.
12. Nishimura M, Scherf S, Behrmann M (2009) Development of object recognition in humans. *F1000 Biol Rep* 1:56.
13. Behrmann M, Williams P (2007) Impairments in part-whole representations of objects in two cases of integrative visual agnosia. *Cogn Neuropsychol* 24(7):701–730.
14. Gilaie-Dotan S, Bentin S, Harel M, Rees G, Saygin AP (2011) Normal form from biological motion despite impaired ventral stream function. *Neuropsychologia* 49(5):1033–1043.
15. Saygin AP (2007) Superior temporal and premotor brain areas necessary for biological motion perception. *Brain* 130(Pt 9):2452–2461.
16. Ahlström V, Blake R, Ahlström U (1997) Perception of biological motion. *Perception* 26(12):1539–1548.
17. Brainard DH (1997) The Psychophysics Toolbox. *Spat Vis* 10(4):433–436.
18. Pelli DG (1997) The VideoToolbox software for visual psychophysics: Transforming numbers into movies. *Spat Vis* 10(4):437–442.
19. Watson AB, Pelli DG (1983) QUEST: A Bayesian adaptive psychometric method. *Percept Psychophys* 33(2):113–120.

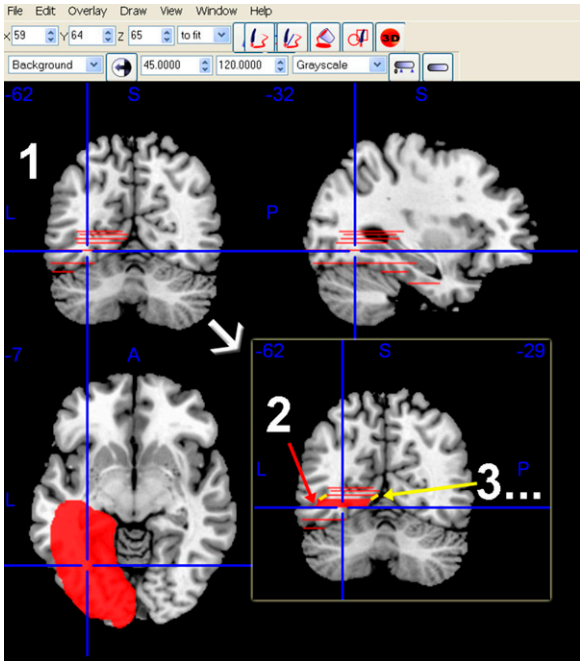

Fig. S1. Demonstration of the filling-in procedure of the traced lesion volume (as was done in the case of GB, EC, and SH). The filling in was achieved by linearly interpolating in the coronal and sagittal planes between the traces of the lesion (in the axial planes, see above *Bottom Left*). One step is shown (in a coronal section) where the interpolation is performed between two traced axial slices (1), and filled in red (2). The step to follow repeats this procedure by filling in the region enclosed by the yellow and red lines (3).

Table S1. Exp. 2 statistical results

	Versus healthy age-matched controls	
Patient	*t*	*P*
EL	0.30	0.77
GB	1.56	0.15*
SH	−0.65	0.53
CR	−1.42	0.18
SM	−0.88	0.39
EC	−0.76	0.46

In Exp. 2, biological motion perceptual thresholds (number of noise points masking the stimuli while performance is at 75% accuracy; see *Methods*) of patients were not significantly different from their age-matched healthy controls. Significance presentation conventions as in Table 2.

Movie S1. A schematic demonstration of Exp. 1. On the left side is a biological motion PLD depicting underarm throwing as in bowling, and on the right side a spatially scrambled version of this animation is presented. Both of these are embedded in additional noise points. Participants had to determine the side of the biological motion (right or left). See main text for further details.

Movie S1

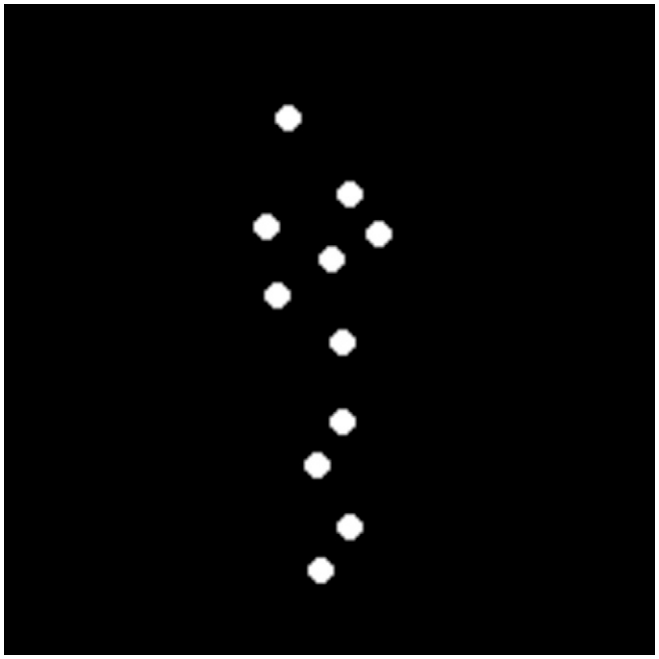

Movie S2. Biological motion animation of throwing, which is one of the seven actions used in Exp. 1.

Movie S2

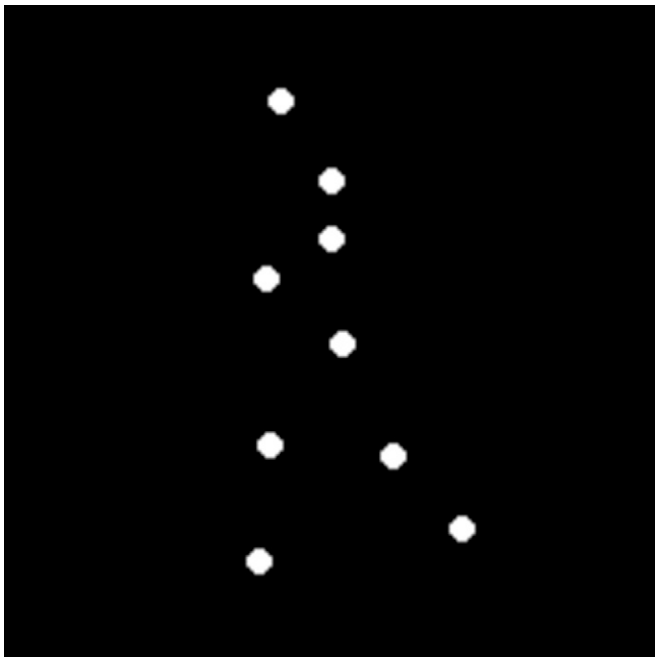

Movie S3. Biological motion animation of a walking upright human figure, which is one of the seven actions used in Exp. 1. This animation was also used in Exp. 2.

Movie S3